Results in Applied Mathematics 10 (2021) 100155

Contents lists available at ScienceDirect

Results in Applied Mathematics

journal homepage: www.elsevier.com/locate/results-in-applied-mathematics

High order finite volume weighted essentially non-oscillatory scheme for solving the isentropic two-phase flow model

Asad Rehman [a], Rana Danish Aslam [b,*], M.A. Meraj [a], Shamsul Qamar [b,c]

[a] Department of Mathematics, University of Education, Lahore, Pakistan
[b] Department of Mathematics, COMSATS University Islamabad, Park Road Chak Shahzad, Islamabad, Pakistan
[c] Max Planck Institute for Dynamics of Complex Technical Systems, Sandtorstrasse 1, 39106 Magdeburg, Germany

ARTICLE INFO

Article history:
Received 9 December 2020
Received in revised form 24 February 2021
Accepted 24 March 2021
Available online xxxx

Keywords:
Two-phase model
WENO scheme
Non-conservative terms
Interfacial pressure
Interfacial velocity
Shock wave

ABSTRACT

This article presents the fifth-order weighted essentially non-oscillatory numerical method for solving a five-equation two-pressure non-conservative model of isentropic two-phase flow. The presence of non-conservative terms, shock waves and contact discontinuities offers more challenging tasks for developing the high order robust numerical methods. The proposed numerical scheme suppresses the unwanted oscillations near the steep gradients and resolves the contact discontinuities in an efficient way. Further, different test problems are taken to validate the efficiency of the proposed numerical scheme. Moreover, the improved central upwind scheme (CUP) is extended to solve the same model for checking the accuracy of the proposed numerical method. The numerical solutions obtained by the suggested scheme are compared with the solution profiles obtained from modified central upwind scheme.

© 2021 The Author(s). Published by Elsevier B.V. This is an open access article under the CC BY license (http://creativecommons.org/licenses/by/4.0/).

1. Introduction

Mathematical modeling and numerical simulation of two-phase flows are currently very dynamic areas of the research. The main reason to study the two-phase flow is its large number of applications in real-life phenomenon [1–4]. Besides the importance of two-phase flow models, the non-hyperbolic character of these models is the main problem that is faced during the modeling of such types of flows. It is well-known fact that the hyperbolicity is the necessary condition for the well-posedness of the mathematical model of the two-phase flows [5]. Further, the authors in this article [5] have analyzed that many of the two-phase flow models with single pressure equation are ill-posed due to the presence of complex-valued characteristics. Thus the researchers take more interest to model and simulate the hyperbolic two-phase flows with separately pressure equations for both phases. The other problem is faced due to the presence of non-conservative terms in the two-phase flow models. Almost all two-phase flow models either with single pressure equation or two pressure equations include the non-conservative terms due to the interface interaction. In literature the prominent non-conservative models with two pressure equations are introduced by Ransom-scofield in 1976 [6], Hicks in 1981 [7], Ransom–Hicks in 1984 [8], Baer-Nunziato in 1986 [9] and Saurel-abgrall in 1999 [10] respectively. Later, the researchers have derived various three to six equations models from the above mentioned models [11–13]. For detail, the reader is referred to the articles [14–18] and references therein.

* Corresponding author.
E-mail address: ranadanish.aslam@gmail.com (R.D. Aslam).

https://doi.org/10.1016/j.rinam.2021.100155
2590-0374/© 2021 The Author(s). Published by Elsevier B.V. This is an open access article under the CC BY license (http://creativecommons.org/licenses/by/4.0/).

Here, five-equation two-pressure model of isentropic two-phase flow [19] is considered. This model is a reduced version of Saurel-abgrall two-phase flow model that was presented in 1999 [10]. The considered model consists of five equations, four of them express the laws of conservation of mass and momentum for gas and liquid phases. The fifth equation expresses the evolution of gas volume fraction with the speed of mean interfacial velocity. Like other two-phase flow models, the considered model also consists of non-conservative terms. These non-conservative terms and hyperbolic nature of the considered model offer difficulties for developing the high order robust numerical schemes. Here, the fifth-order finite volume WENO [20] and the second-order high resolution central upwind schemes [21] are developed for solving the considered model. Initially, a theoretical solution and upwind non-conservative methods were proposed to solve the considered model by Castro and Toro in the article [19]. They used the Monotonic Upstream-centered Scheme for Conservation Laws (MUSCL) and Arbitrary accuracy Derivatives Riemann problem (ADER) approaches for developing the second-order non-conservative numerical methods.

In this article, fifth-order finite volume WENO numerical scheme [20] is developed for solving the unsteady isentropic five-equation two-pressure model. Before applying the finite volume WENO scheme, we rewrite the fifth equation of a considered model in a more compatible way to our numerical scheme as described in Section 2. The proposed numerical scheme is more simple and entirely different as compare to the numerical schemes that were designed to solve the considered model in the article [19]. Initially, the third-order finite volume WENO numerical scheme was presented by Liu et al. [22] in 1994 that was improved version of essentially non-oscillatory (ENO) numerical scheme [23–25]. In this version of finite volume WENO scheme, they improved the order of accuracy and used the convex combination of all the candidate stencils. Since then, these numerical schemes are being developed, modified and extended for different fields of science and engineering, for detail see [26–34] and the references therein. The proposed numerical scheme resolves the sharp discontinuities efficiently and ensures high order accuracy in the smooth regions.

The remaining article is organized as follow. In Section 2, the mathematical form of the isentropic two-phase flow model and eigenvalues of the considered model are given. The finite volume WENO numerical method for the considered model is derived in Section 3. In Section 4, the number of test problems are considered to validate and compare the results of proposed numerical method with the improved central upwind numerical method [21]. Finally, in Section 5, the conclusions are presented.

2. Isentropic two-phase flow model

This section presents the mathematical form and eigenvalues of the isentropic two-phase flow non-conservative model. The fundamental equations for the considered model are given as follow

$$\begin{aligned}
&\frac{\partial}{\partial t}(a_l\rho_l)+\frac{\partial}{\partial x}(a_l\rho_l u_l)=0,\\
&\frac{\partial}{\partial t}(a_g\rho_g)+\frac{\partial}{\partial x}(a_g\rho_g u_g)=0,\\
&\frac{\partial}{\partial t}(a_l\rho_l u_l)+\frac{\partial}{\partial x}(a_l\rho_l u_l^2+a_l p_l)=-p_i\frac{\partial}{\partial x}(a_g),\\
&\frac{\partial}{\partial t}(a_g\rho_g u_g)+\frac{\partial}{\partial x}(a_g\rho_g u_g^2+a_g p_g)=p_i\frac{\partial}{\partial x}(a_g),\\
&\frac{\partial}{\partial t}(a_g)+u_i\frac{\partial}{\partial x}(a_g)=0.
\end{aligned} \tag{1}$$

Here, ρ_l and ρ_g are densities, a_g and a_l present the volume-fractions, u_l and u_g denote velocities and p_l and p_g are pressures. Where subscripts g and l represent the gas and liquid phases respectively. Further, p_i and u_i represent the interface pressure and interface velocity respectively. The same expressions are taken for the p_i and u_i as given in the article [19], which are

$$p_i=(a_l p_l+a_g p_g)\ \text{ and }\ u_i=\frac{(a_l\rho_l u_l+a_g\rho_g u_g)}{(a_l\rho_l+a_g\rho_g)} \tag{2}$$

The last equation of the model (1) represents the evolution of volume fraction. In this article, we rewrite this equation as follow

$$\partial_t(a_g)+\partial_x(a_g u_i)=a_g\partial_x(u_i). \tag{3}$$

The model (1) consists eight unknowns ρ_l, ρ_g, u_l, u_g, p_l, p_g, a_l, a_g and five equations. Thus to close the system additional constraints are needed. These additional constraints are given as follow

1. Volume-fractions are related by the following relation

$$a_l+a_g=1. \tag{4}$$

Table 1
Parameters used in numerical computation of the five equation two pressure model.

Parameters	Value
ρ_0	10^3 kg/m^3
k_g	10^5 Pa
k_l	3.03975×10^8 Pa
γ_l	7.15
γ_g	1.4

2. The liquid phase pressure is defined by using the Tait's equation of state [19]

$$p_l = k_l \left(\left(\frac{\rho_l}{\rho_0} \right)^{\gamma_l} - 1 \right), \tag{5}$$

and gas phase pressure is defined

$$p_g = k_g (\rho_g)^{\gamma_g}. \tag{6}$$

Here $\rho_0, k_g, k_l, \gamma_l$ and γ_g are constant parameters and values are given in Table 1.

2.1. Eigenvalues

The considered model (1) with the help of Eq. (3) can be written in the form

$$\partial_t W + \partial_x F(W) = S(W), \tag{7}$$

where

$$W = \begin{pmatrix} a_l\rho_l \\ a_g\rho_g \\ a_l\rho_l u_l \\ a_g\rho_g u_g \\ a_g \end{pmatrix}, \quad F(W) = \begin{pmatrix} a_l\rho_l u_l \\ a_g\rho_g u_g \\ a_l\rho_l u_l^2 + a_l p_l \\ a_g\rho_g u_g^2 + a_g p_g \\ u_i a_g \end{pmatrix}, S(W) = \begin{pmatrix} 0 \\ 0 \\ -p_i\partial_x(a_g) \\ p_i\partial_x(a_g) \\ a_g\partial_x(u_i) \end{pmatrix},$$

with $W = (w_1,\ w_2,\ w_3,\ w_4,\ w_5) = (a_l\rho_l,\ a_g\rho_g,\ a_l\rho_l u_l,\ a_g\rho_g u_g,\ a_g)$, $F(W) = (f_1,\ f_2,\ f_3,\ f_4,\ f_5) = (a_l\rho_l u_l,\ a_g\rho_g u_g,\ a_l\rho_l u_l^2 + a_l p_l,\ a_g\rho_g u_g^2 + a_g p_g,\ a_g u_i)$ and $S(W) = (s_1, s_2, s_3, s_4, s_5)$. Now, the Eq. (7) can be rewritten as

$$\partial_t \begin{pmatrix} w_1 \\ w_2 \\ w_3 \\ w_4 \\ w_5 \end{pmatrix} + \partial_x \begin{pmatrix} w_3 \\ w_4 \\ \frac{w_3^2}{w_1} + p_l(w_1) \\ \frac{w_4^2}{w_2} + p_g(w_2) \\ w_5(\frac{(w_3+w_4)}{(w_1+w_2)}) \end{pmatrix} = \begin{pmatrix} 0 \\ 0 \\ s_3 \\ s_4 \\ s_5 \end{pmatrix}. \tag{8}$$

Now, the speeds of sound for gas and liquid phases can be found as

$$c_g = \sqrt{\left(\frac{\gamma_g p_g}{\rho_g} \right)}, \quad c_l = \sqrt{\left(\frac{\gamma_l (p_l + k_l)}{\rho_l} \right)}. \tag{9}$$

Hence, the eigenvalues for the considered system are

$$\lambda_1 = u_l - c_l, \lambda_2 = u_g - c_g, \lambda_3 = u_i, \lambda_4 = u_l + c_l, \lambda_5 = u_g + c_g. \tag{10}$$

The considered model has real and distinct eigenvalues and it is strictly hyperbolic as c_l and c_g are strictly greater than zero.

3. Construction of fifth-order WENO numerical scheme for considered model

This section presents the construction of finite volume WENO numerical scheme for approximating the isentropic two phase flow model. As the considered model can be written in a compact form as follow

$$\partial_t W + \partial_x F(W) = S(W, x), \quad t > 0, x \in \Omega, \tag{11}$$

and divide the domain Ω into cells $C_i = [x_{i-\frac{1}{2}}, x_{i+\frac{1}{2}}], i = 1, \ldots, N$. Here, the center of ith cell is denoted by $x_i = \frac{\left(x_{i-\frac{1}{2}} + x_{i+\frac{1}{2}}\right)}{2}$ and length of ith cell by $\triangle x_i$. By integrating the Eq. (11) over C_i, we have

$$\frac{d}{dt}W_i(t) + \frac{1}{\triangle x_i}\left(F(W(x_{i+\frac{1}{2}}, t) - F(W(x_{i-\frac{1}{2}}, t))\right) = \frac{1}{\triangle x_i}\int_{x_{i-\frac{1}{2}}}^{x_{i+\frac{1}{2}}} S(W, x)dx, \tag{12}$$

where $W_i(t) = \frac{1}{\triangle x_i}\int_{x_{i-\frac{1}{2}}}^{x_{i+\frac{1}{2}}} W(x, t)dx$. The Eq. (12) can be approximated as follow

$$\frac{d}{dt}W_i(t) + \frac{1}{\triangle x_i}\left(\hat{F}_{i+\frac{1}{2}} - \hat{F}_{i-\frac{1}{2}}\right) = \frac{1}{\triangle x_i}\int_{x_{i-\frac{1}{2}}}^{x_{i+\frac{1}{2}}} S(W, x)dx. \tag{13}$$

Where, $\hat{F}_{i+\frac{1}{2}} = \mathcal{F}\left(W^-_{i+\frac{1}{2}}, W^+_{i+\frac{1}{2}}\right)$ denotes the monotone numerical flux and $W^{\pm}_{i+\frac{1}{2}}$ are pointwise approximations to $W(x_{i+\frac{1}{2}}, t)$. Here, we will use the Lax–Friedrichs flux (LFF) as a monotone numerical flux which is defined as below

$$\mathcal{F}\left(W^-_{i+\frac{1}{2}}, W^+_{i+\frac{1}{2}}\right) = \frac{1}{2}\left(F(W^-_{i+\frac{1}{2}}) + F(W^+_{i+\frac{1}{2}}) - \vartheta(W^+_{i+\frac{1}{2}} - W^-_{i+\frac{1}{2}})\right), \tag{14}$$

where $\vartheta = \max_W |F'(W)|$. Now computational variables are $W_i(t)$ which will approximate the cell-averages $W(x_i, t)$. Further, the $W^-_{i+\frac{1}{2}}$ and $W^+_{i+\frac{1}{2}}$ are calculated through the adjacent cell-average values W_i by WENO reconstruction. The point-wise reconstructed values $W^+_{i+\frac{1}{2}}$ and $W^-_{i+\frac{1}{2}}$ are obtained by the following relations

$$W^+_{i+\frac{1}{2}} = \omega_1\hat{W}^1_{i+\frac{1}{2}} + \omega_2\hat{W}^2_{i+\frac{1}{2}} + \omega_3\hat{W}^3_{i+\frac{1}{2}}, \tag{15}$$

$$W^-_{i+\frac{1}{2}} = \tilde{\omega}_1\tilde{W}^1_{i+\frac{1}{2}} + \tilde{\omega}_2\tilde{W}^2_{i+\frac{1}{2}} + \tilde{\omega}_2\tilde{W}^2_{i+\frac{1}{2}}, \tag{16}$$

where $\hat{W}^l_{i+\frac{1}{2}}$ and $\tilde{W}^l_{i-\frac{1}{2}}$, for $l = 1, 2, 3$, are reconstructed values and defined as

$$\hat{W}^1_{i+\frac{1}{2}} = \frac{1}{6}\left(2W^+_i + 5W^+_{i+1} - W^+_{i+2}\right), \tag{17}$$

$$\hat{W}^2_{i+\frac{1}{2}} = \frac{1}{6}\left(-W^+_{i-1} + 5W^+_i + 2W^+_{i+1}\right), \tag{18}$$

$$\hat{W}^3_{i+\frac{1}{2}} = \frac{1}{6}\left(2W^+_{i-2} - 7W^+_{i-1} + 11W^+_i\right), \tag{19}$$

and

$$\tilde{W}^1_{i+\frac{1}{2}} = \frac{1}{6}\left(11W^-_{i+1} - 7W^-_{i+2} + W^-_{i+3}\right), \tag{20}$$

$$\tilde{W}^2_{i+\frac{1}{2}} = \frac{1}{6}\left(W^-_i + 5W^-_{i+1} - W^-_{i+2}\right), \tag{21}$$

$$\tilde{W}^3_{i+\frac{1}{2}} = \frac{1}{6}\left(-W^-_{i-1} + 5W^-_{i-1} + W^-_i\right). \tag{22}$$

The nonlinear weights ω_l and $\tilde{\omega}_l$ in Eqs. (15) and (16) are defined as

$$\omega_l = \frac{\xi_l}{\sum_{m=1}^{3}\xi_m} \quad \text{with} \quad \xi_l = \frac{\sigma_l}{\epsilon + \mathfrak{B}_l}, \quad l = 1, 2, 3, \tag{23}$$

and

$$\tilde{\omega}_l = \frac{\tilde{\xi}_l}{\sum_{m=1}^{3}\tilde{\xi}_m} \quad \text{with} \quad \tilde{\xi}_l = \frac{\tilde{\sigma}_l}{\varepsilon + \tilde{\mathfrak{B}}_l}, \quad l = 1, 2, 3, \tag{24}$$

Here ε can be taken any small positive number for avoiding the denominator to become zero and we set $\varepsilon = 10^{-7}$ in all the simulations. Here, σ_l and $\tilde{\sigma}_l$ represent the linear weights and $\mathfrak{B}_l$ and $\tilde{\mathfrak{B}}_l$ denote the smoothness indicators. The values

of σ_l and $\tilde{\sigma}_l$ are given as

$$\sigma_l = \begin{cases} \frac{3}{10} \text{ if } l = 1, \\ \frac{6}{10} \text{ if } l = 2, \\ \frac{1}{10} \text{ if } l = 3, \end{cases} \quad \text{and} \quad \tilde{\sigma}_l = \begin{cases} \frac{1}{10} \text{ if } l = 1, \\ \frac{6}{10} \text{ if } l = 2, \\ \frac{3}{10} \text{ if } l = 3. \end{cases} \tag{25}$$

The values of smoothness indicators $\mathfrak{B}_l$ and $\tilde{\mathfrak{B}}_l$ are defined as

$$\mathfrak{B}_l = \begin{cases} \frac{13}{12}\left(W_i^+ - 2W_{i+1}^+ + W_{i+2}^+\right)^2 + \frac{1}{4}\left(W_i^+ - 4W_{i+1}^+ + W_{i+2}^+\right)^2 \text{ if } l = 1, \\ \frac{13}{12}\left(W_{i-1}^+ - 2W_i^+ + W_{i+1}^+\right)^2 + \frac{1}{4}\left(W_{i-1}^+ - W_{i+1}^+\right)^2 \text{ if } l = 2, \\ \frac{13}{12}\left(W_{i-2}^+ - 2W_{i-1}^+ + W_i^+\right)^2 + \frac{1}{4}\left(W_{i-2}^+ - 4W_{i-1}^+ + W_i^+\right)^2 \text{ if } l = 3. \end{cases} \tag{26}$$

and

$$\tilde{\mathfrak{B}}_l = \begin{cases} \frac{13}{12}\left(W_{i+1}^- - 2W_{i+2}^- + W_{i+3}^-\right)^2 + \frac{1}{4}\left(3W_{i+1}^- - 4W_{i+2}^- + W_{i+3}^-\right)^2 \text{ if } l = 1, \\ \frac{13}{12}\left(W_i^- - 2W_{i+1}^- + W_{i+2}^-\right)^2 + \frac{1}{4}\left(W_i^- - W_{i+2}^-\right)^2 \text{ if } l = 2, \\ \frac{13}{12}\left(W_{i-1}^- - 2W_i^- + W_{i+1}^-\right)^2 + \frac{1}{4}\left(W_{i-1}^- - 4W_i^- + 3W_{i+1}^-\right)^2 \text{ if } l = 3. \end{cases} \tag{27}$$

This completes the procedure of spatial reconstruction. Next, we discretize the nonzero terms on the right hand side of the Eq. (7).

$$\int_{x_{i-\frac{1}{2}}}^{x_{i+\frac{1}{2}}} s_3 dx = \int_{x_{i-\frac{1}{2}}}^{x_{i+\frac{1}{2}}} (-p_i \partial_x(a_g)) dx \tag{28}$$

$$= -(\bar{p_i})\left((a_g)_{i+\frac{1}{2}} - (a_g)_{i-\frac{1}{2}}\right) \tag{29}$$

Here, $\bar{p_i}$ is the averaged value at the cell C_i and $(a_g)_{i\pm\frac{1}{2}}$ are the source fluxes at the interfaces of the cell C_i. Further, for the right interface of C_i, we write as

$$(a_g)_{i+\frac{1}{2}} = (a_g)_i^+ + (a_g)_{i+1}^- \tag{30}$$

Similarly, the values of left interface of the cell C_i and discretization of $\int_{x_{i-\frac{1}{2}}}^{x_{i+\frac{1}{2}}} s_4$ and $\int_{x_{i-\frac{1}{2}}}^{x_{i+\frac{1}{2}}} s_5$ are obtained. Further, S_i denotes the approximation of the expression $\int_{x_{i-\frac{1}{2}}}^{x_{i+\frac{1}{2}}} S(W, x)dx$. Finally, we end up with the semi-discrete equation as follow

$$\frac{d}{dt}\overline{W}_i(t) = -\frac{1}{\triangle x_i}\left(\hat{F}_{i+\frac{1}{2}} - \hat{F}_{i-\frac{1}{2}}\right) + \frac{1}{\triangle x_i} S_i, \tag{31}$$

or the above equation can be written as

$$\frac{d}{dt}\overline{W}_i(t) = \mathcal{O}(W). \tag{32}$$

Now, for solving the system of ordinary differential Eq. (32), we apply the third-order TVD RK method [20] as follow

$$\begin{aligned} W^{(1)} &= W^n + dt\mathcal{O}(W^n), \\ W^{(2)} &= \frac{3}{4}W^n + \frac{1}{4}\left(W^{(1)} + dt\mathcal{O}(W^{(1)})\right), \\ W^{(n+1)} &= \frac{1}{3}W^n + \frac{2}{3}\left(W^{(2)} + dt\mathcal{O}(W^{(2)})\right), \end{aligned} \tag{33}$$

where $\mathcal{O}(W)$ is the spatial operator. The time step dt is estimated by using the relation $\frac{CFL*dx}{\max(|\lambda_1|,|\lambda_2|,|\lambda_3|,|\lambda_4|,|\lambda_5|)}$, where CFL denotes the Courant–Friedrichs–Lewy condition.

4. Numerical test problems

This section presents different types of test problems for the five-equation two-phase flow model. Both WENO and modified central upwind numerical schemes [21] are applied to simulate the two phase flows. The numerical solutions obtained from the WENO scheme are compared with the solutions obtained from the central upwind numerical scheme. All test problems are taken from [19].

Test Problem 1: In this test problem, the numerical solutions are obtained in the computational domain [0, 1] and initial discontinuity is located at $x = 0.5$. The computational domain is divided into 400 grid points. The left and right states for

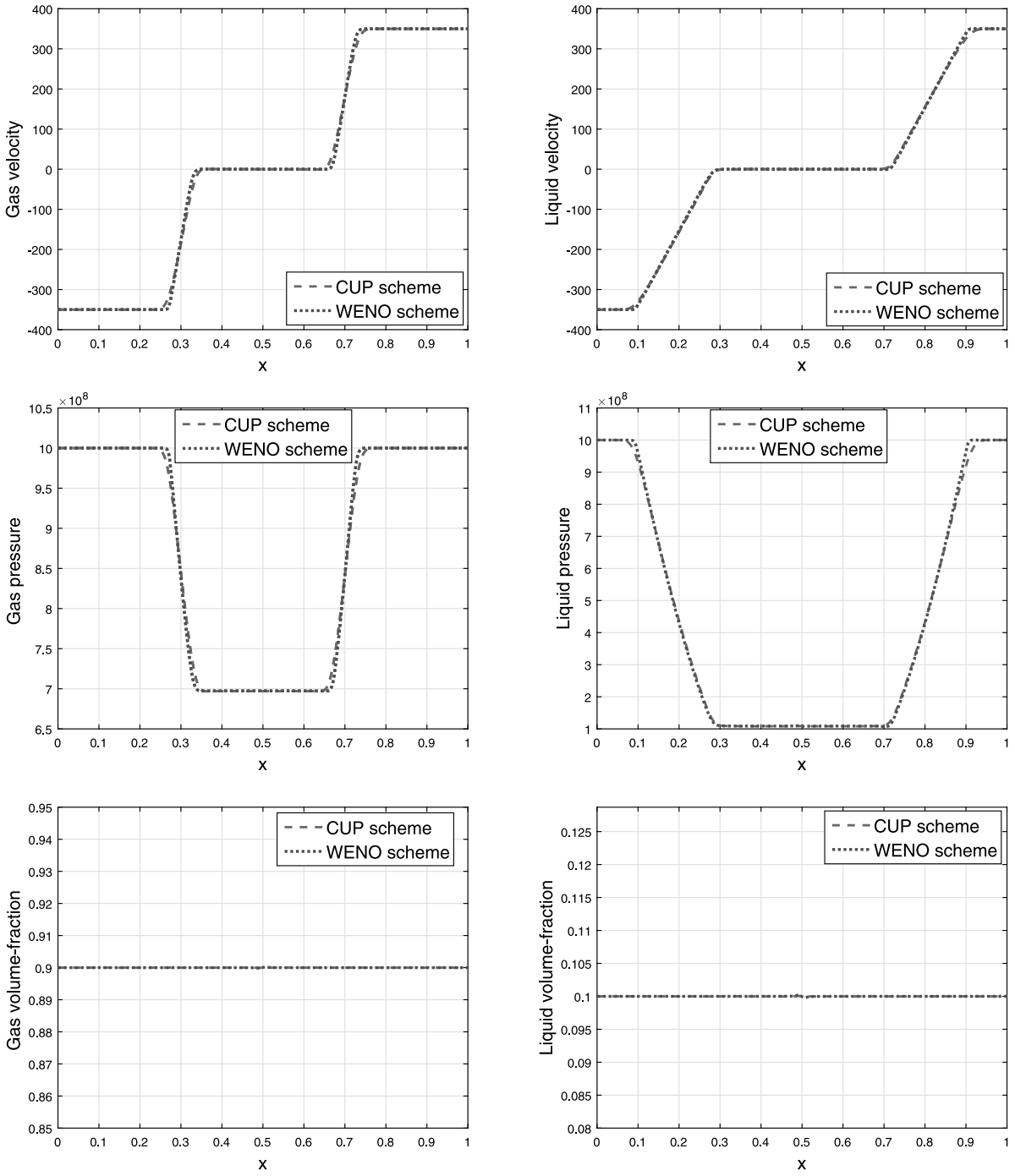

Fig. 1. The numerical solutions obtained at $t = 1.3 \times 10^{-4}$ by WENO and CUP schemes.

this Riemann problem are considered as

$$(\rho_g, \rho_l, u_g, u_l, \alpha_g, \alpha_l)(x, 0) = \begin{cases} (719.6856, 1225.8912, -350, -350, 0.9), & x < 0.5, \\ (719.6856, 1225.8912, 350, 350, 0.9), & x > 0.5. \end{cases} \tag{34}$$

The solution profiles for the gas velocity, liquid velocity, gas pressure, liquid pressure, gas volume-fraction and liquid volume-fraction are obtained at $t = 1.3 \times 10^{-4}$ and are given in Fig. 1. The numerical solution comprises four symmetric rarefaction waves and a trivial contact discontinuity. The proposed and modified central upwind numerical schemes have

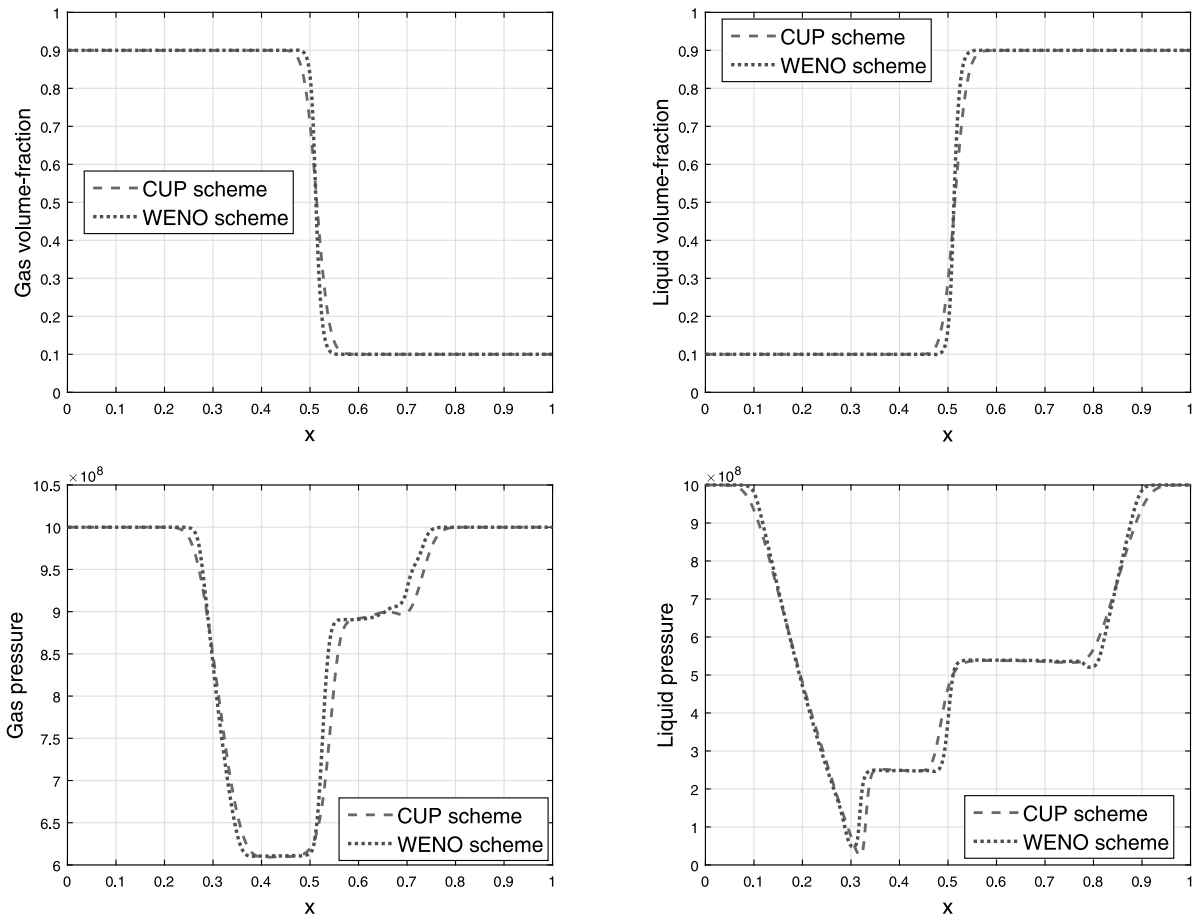

Fig. 2. Comparison of the numerical results obtained by finite volume WENO and CUP schemes.

good agreement with each other as there is no discontinuity in the solution domain. Even though the solution profiles for the gas and liquid pressures show that the finite volume WENO numerical scheme is less diffusive as compare to modified central upwind scheme.

Test Problem 2: This test problem is considered for checking the accuracy of the considered numerical schemes. For this test problem the solution domain consists the sharp discontinuity. The system is subjected to the following initial conditions

$$(\rho_g, \rho_l, u_g, u_l, \alpha_g, \alpha_l)(x,0) = \begin{cases} (719.6856, 1225.8912, -350, -250, 0.9), & x < 0.5, \\ (719.6856, 1225.8912, 350, 250, 0.1), & x > 0.5. \end{cases} \tag{35}$$

The solution profiles for gas volume fraction, liquid volume-fraction,gas pressure and liquid pressure are obtained at $t = 1.3 \times 10^{-4}$ and shown in Fig. 2. The solution domain for this Riemann problem consists of the four rarefaction waves and a non-trivial contact discontinuity. Despite the presence of sharp discontinuity, both numerical schemes do not produce the unwanted oscillations near the sharp discontinuity.

Test problem 3: This test problem is considered for checking the efficiency and accuracy of the derived numerical schemes. In this problem, the computational domain [0, 1] is discretized into 800 grid points. The initial conditions are considered as follow respectively.

$$(\rho_g, \rho_l, u_g, u_l, \alpha_g, \alpha_l)(x,0) = \begin{cases} (719.6856, 1225.8912, 150, 150, 0.9), & x < 0.5, \\ (719.6856, 1225.8912, -150, -150, 0.9), & x > 0.5. \end{cases} \tag{36}$$

The numerical solutions for the gas velocity, liquid velocity, gas pressure and liquid pressure are computed at time $t = 1.3 \times 10^{-4}$ and given in Fig. 3. The solution domain consists of four weak shock waves and a trivial contact discontinuity. The proposed numerical scheme resolved the discontinuities in a very efficient way, as shown in Fig. 3. The solution profiles for liquid velocity and liquid pressure show that the WENO scheme captures the constant states

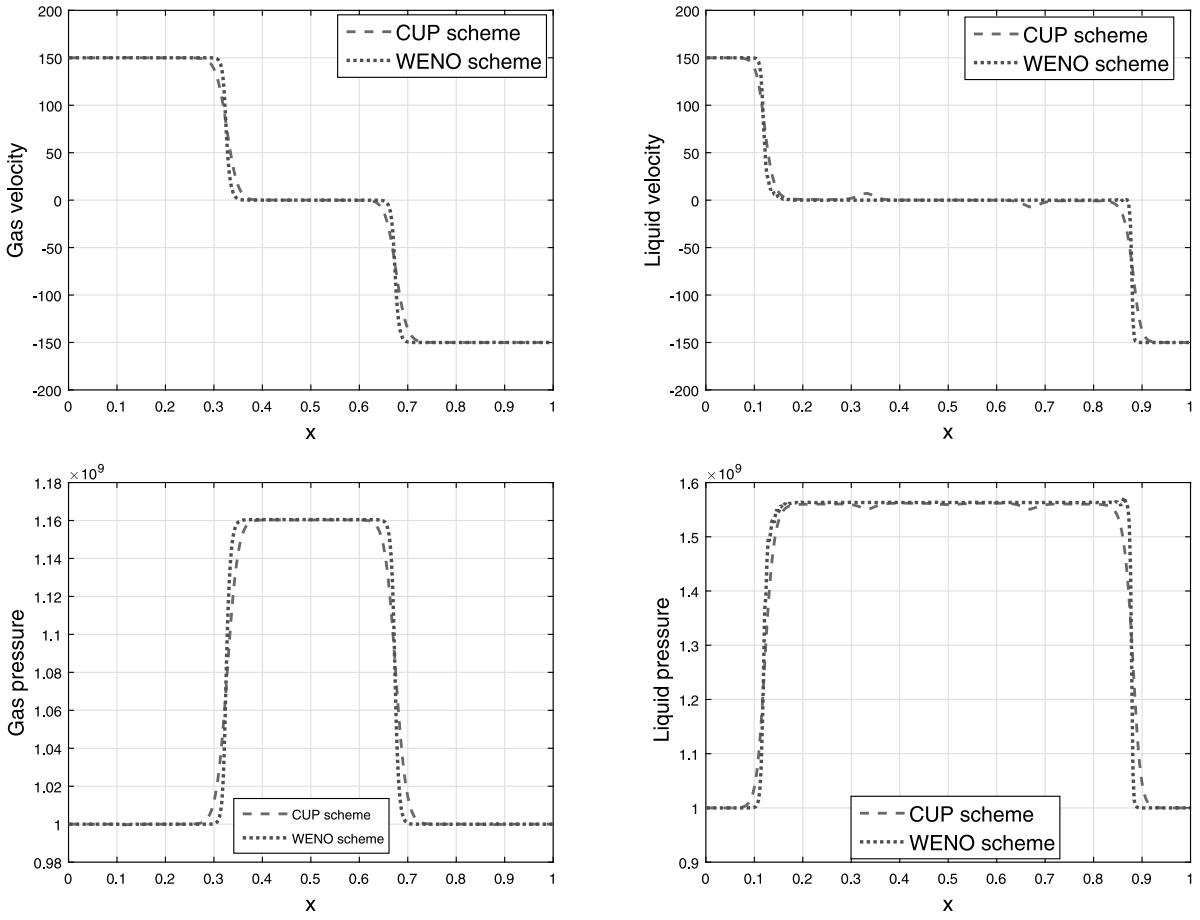

Fig. 3. Comparison of the numerical results obtained by finite volume WENO and CUP schemes.

more efficiently as compare to the modified central upwind scheme. The central upwind scheme produces two humps near $x = 0.3$ and $x = 0.7$ in above mentioned solution profiles.

Test problem 4: This test problem is considered for checking the efficiency of considered numerical schemes as the solution domain consists of a sonic point. The initial conditions for this Riemann problem are given as

$$(\rho_g, \rho_l, u_g, u_l, \alpha_g, \alpha_l)(x, 0) = \begin{cases} (719.6856, 1225.8912, 1000, 2400., 0.9), & x < 0.5, \\ (261.5970, 2277.81, 1028.3588, 2774.36, 0.9), & x > 0.5. \end{cases} \tag{37}$$

The solution profiles for gas velocity, liquid velocity, gas pressure,liquid pressure, gas density and liquid density are obtained at time $t = 4.0 \times 10^{-4}$ and shown in Fig. 4. Further, the computational domain is divided into 300 grid points. The solution domain consists of a single isolated rarefaction wave. As we know that the sonic flows offer difficulties for the numerical methods in the form of entropy glitch. The proposed numerical schemes handle the sonic point in an efficient way.

For the next two problems, taken from the article [35], we will add some terms in the right hand side of the Eq. (7). Now, the term $S(W)$ in Eq. (7) is defined as follow

$$S(W) = \begin{pmatrix} 0 \\ 0 \\ -p_i \partial_x(a_g) + a_l \rho_l g + F_D \\ p_i \partial_x(a_g) + a_g \rho_g g + F_D \\ a_g \partial_x(u_i) + \frac{v_i}{H} \end{pmatrix}.$$

Here, $g(= 9.81)$, F_D and v_i represent the gravity, drag force and interface velocity. Further, the drag force and interface velocity are defined as $F_D = C_d(u_g - u_l)$ and $v_i = \frac{p_g - p_l}{a_l + a_g}$, where C_d is the drag coefficient and $a_k = \rho_k c_k$, $k = \{l, g\}$. Note that,

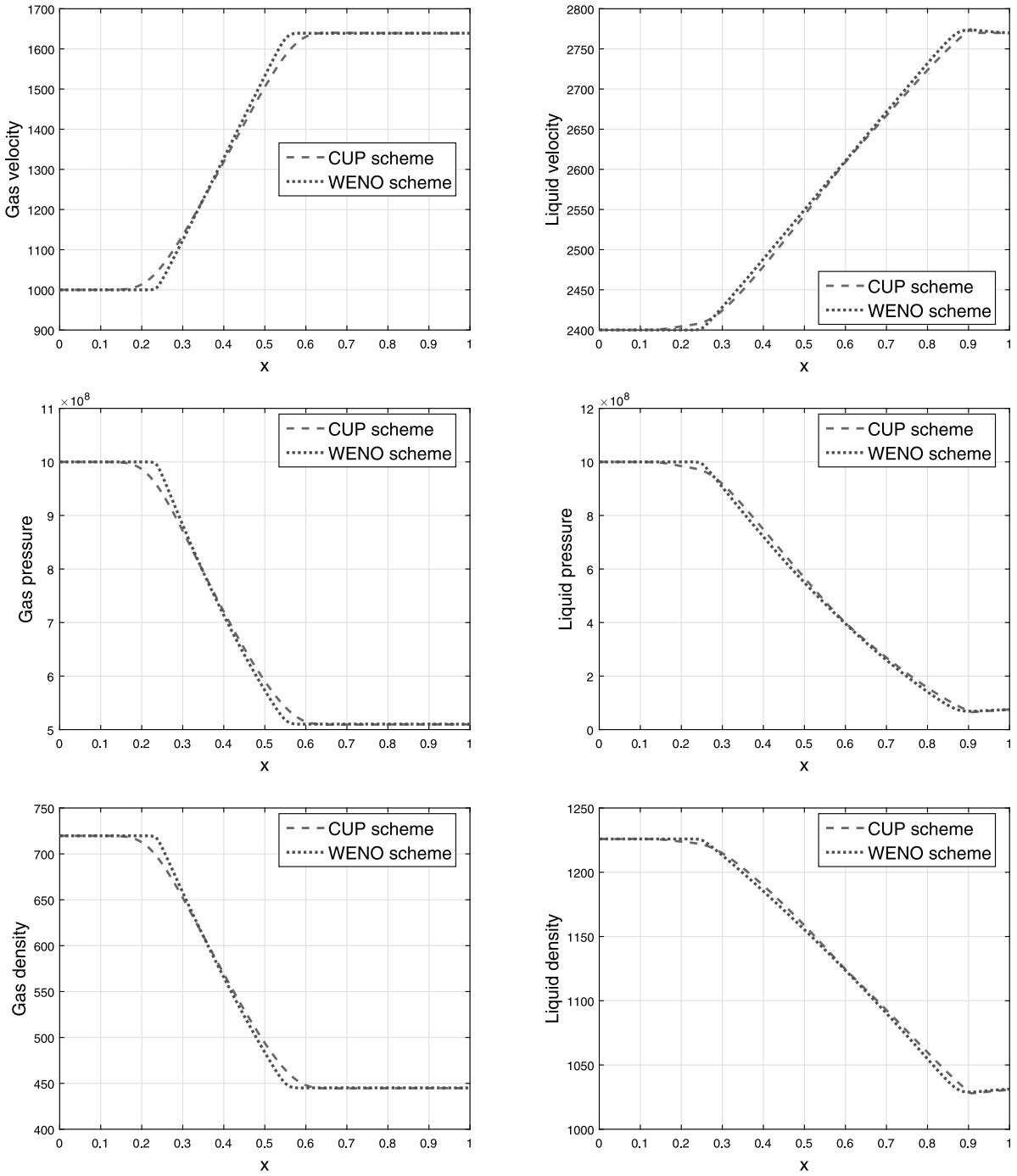

Fig. 4. Numerical solutions obtained by finite volume WENO and CUP scheme at $t = 1.3 \times 10^{-4}$ s.

the drag force is only considered for the sedimentation test problem. For more detail about these problems, the reader is referred to [35] and references therein.

Test problem 5: This test problem is known as one dimensional water-faucet problem and initially introduced by Ransom [36]. In this test problem, 12 m long vertical pipe is considered that is initially filled with 80% liquid and 20% gas. Initially, the liquid and gas velocities are 10 m/s and 0 m/s respectively. The solution profiles of void-fraction and

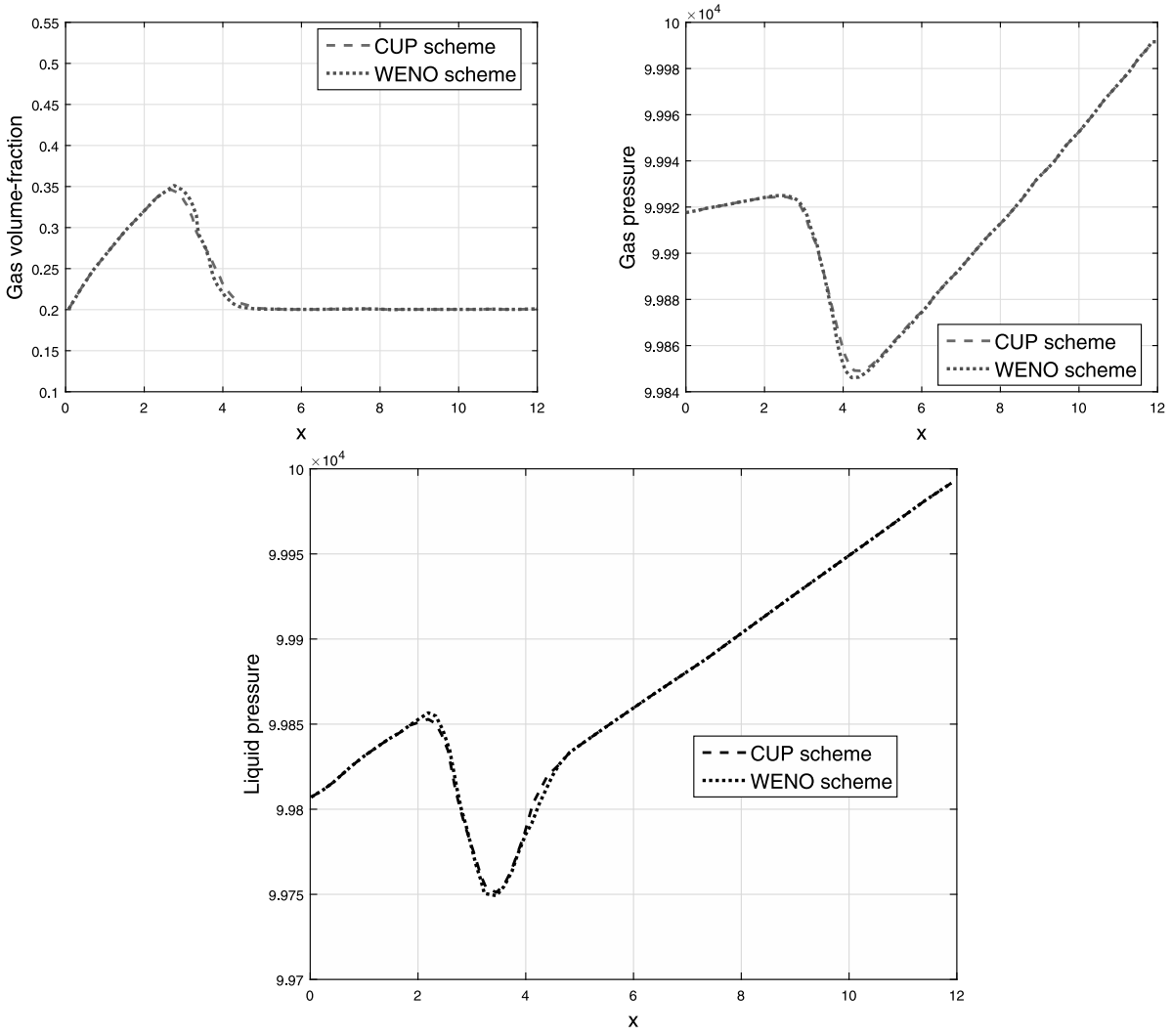

Fig. 5. Numerical solutions obtained by finite volume WENO and CUP scheme at $t = 0.4$ s.

pressures at $t = 0.4$ s are obtained by using the value of $(1/H) = 20\,000$, as given in Fig. 5. The results obtained by considered numerical schemes show good agreement with available results in [35].

Test problem 6: This test problem is known as sedimentation problem and initially introduced by Youngs [36]. Here, the length of vertical pipe is taken 2 m long. Initially, the pipe is filled with a uniform two-phase mixture. Later, the two phases will gradually split into two single-phase zones because of the gravity effect. The solution profiles of void-fraction and pressures at $t = 10$ s are obtained by setting the value of $(1/H) = 20\,000$, as given in Fig. 6. The solution profiles are closely matched with the results obtained by the authors in [35]. Hence, for extensive detail about the Test problems 5 and 6, the reader is referred to [35].

5. Conclusions

In this article, the finite volume WENO numerical scheme was developed to obtain the numerical solutions of the unsteady isentropic two-phase flow model. Despite, the presence of non-conservative terms in the considered model and the presence of shock waves, volume fraction contact discontinuities and sonic point in the solution domains of different test problems, the designed high order numerical scheme resolved the contact discontinuities efficiently, did not create the unwanted oscillations near the shock waves and also did not affect by the presence of sonic point. The robustness of proposed numerical method was checked by considering the different test problems. Further, the numerical solutions obtained by using high order WENO scheme were compared with the solutions those obtained by the CUP numerical scheme. Overall the performance of the designed numerical scheme was better than the high-resolution central upwind numerical scheme.

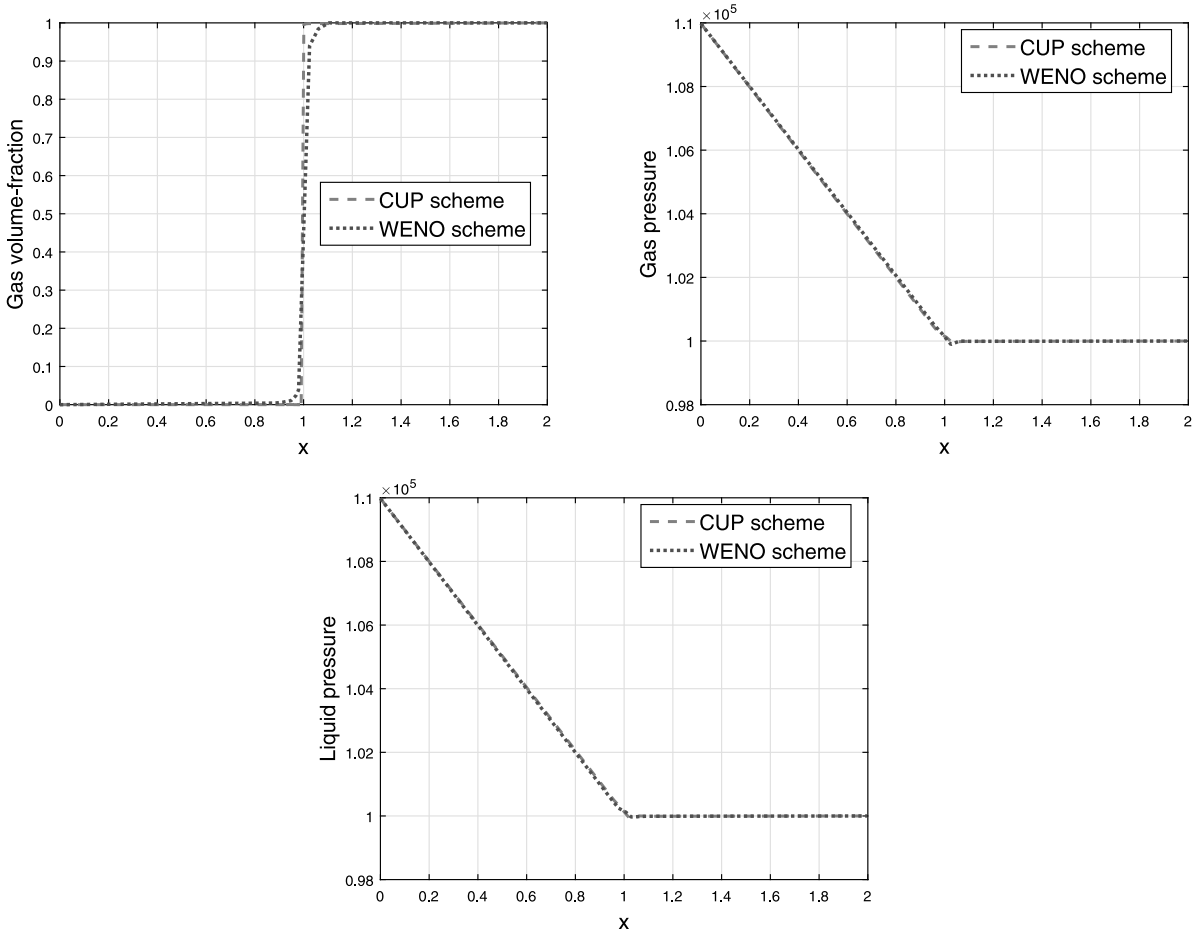

Fig. 6. Numerical solutions obtained by finite volume WENO and CUP scheme at $t = 10$ s.

Declaration of competing interest

The authors declare that they have no known competing financial interests or personal relationships that could have appeared to influence the work reported in this paper.

References

[1] Kapila AK, Menikoff R, Bdzil JB, Son SF, Stewart DS. Two-phase modeling of deflagration-to-detonation transition in granular materials: Reduced equations. Phys Fluids 2001;13(10):3002–24.
[2] Andrianov N, Warnecke G. The Riemann problem for the Baer–Nunziato two-phase flow model. J Comput Phys 2004;195(2):434–64.
[3] Hasan AR, Kabir CS, Sayarpour M. Simplified two-phase flow modeling in wellbores. J Pet Sci Eng 2010;72(1–2):42–9.
[4] Medvedev AE, Fomin VM. Two-phase blood-flow model in large and small vessels. Doklady Phys 2011;56(12):610–3.
[5] Lyczkowski RW, Gidaspow D, Solbrig CW, Hughes ED. Characteristics and stability analyses of transient one-dimensional two-phase flow equations and their finite difference approximations. Nucl Sci Eng 1978;66(3):378–96.
[6] Ransom VH, Scofield MP. Two-pressure hydrodynamic model for two-phase separated flow. In: Idaho National Engineering Laboratory, SRD-50-76. 1976.
[7] Hicks DL. Hyperbolic models for two-phase (or two-material) flow. In: STIN, Vol. 82. 1981, p. 26624.
[8] Ransom VH, Hicks DL. Hyperbolic two-pressure models for two-phase flow. J Comput Phys 1984;53(1):124–51.
[9] Baer MR, Nunziato JW. A two-phase mixture theory for the deflagration-to-detonation transition (DDT) in reactive granular materials. Int J Multiph Flow 1986;12(6):861–89.
[10] Saurel R, Abgrall R. A multiphase Godunov method for compressible multifluid and multiphase flows. J Comput Phys 1999;150(2):425–67.
[11] Van Brummelen EH, Koren B. A pressure-invariant conservative godunov-type method for barotropic two-fluid flows. J Comput Phys 2003;185(1):289–308.
[12] Kreeft JJ, Koren B. A new formulation of Kapila's five-equation model for compressible two-fluid flow, and its numerical treatment. J Comput Phys 2010;229(18):6220–42.
[13] Saurel R, Petitpas F, Berry RA. Simple and efficient relaxation methods for interfaces separating compressible fluids, cavitating flows and shocks in multiphase mixtures. J Comput Phys 2009;228(5):1678–712.

[14] Rehman A, Qamar S. High order finite-volume WENO scheme for five-equation model of compressible two-fluid flow. Comput Math Appl 2018;76(11–12):2648–64.
[15] Abgrall R, Karni S. A comment on the computation of non-conservative products. J Comput Phys 2010;229(8):2759–63.
[16] Gavrilyuk S, Saurel R. Mathematical and numerical modeling of two-phase compressible flows with micro-inertia. J Comput Phys 2002;175(1):326–60.
[17] Sukamta S. Computational fluid dynamics (CFD) and experimental study of two-phase flow patterns gas-liquid with low viscosity in a horizontal capillary pipe. CFD Lett 2019;11:16–23.
[18] Yang S, Yi P, Habchi C. Real-fluid injection modeling and LES simulation of the ECN Spray A injector using a fully compressible two-phase flow approach. Int J Multiph Flow 2020;122:103145.
[19] Castro CE, Toro EF. A Riemann solver and upwind methods for a two-phase flow model in non-conservative form. Internat J Numer Methods Fluids 2006;50(3):275–307.
[20] Shu CW. High-order finite difference and finite volume WENO schemes and discontinuous Galerkin methods for CFD. Int J Comput Fluid Dyn 2003;17(2):107–18.
[21] Kurganov A, Lin CT. On the reduction of numerical dissipation in central-upwind schemes. Commun Comput Phys 2007;2(1):141–63.
[22] Liu XD, Osher S, Chan T. Weighted essentially non-oscillatory schemes. J Comput Phys 1994;115(1):200–12.
[23] Harten A, Osher S. Uniformly high-order accurate nonoscillatory schemes. I. SIAM J Numer Anal 1987;24(2):279–309.
[24] Shu CW, Osher S. Efficient implementation of essentially non-oscillatory shock-capturing schemes. J Comput Phys 1988;77(2):439–71.
[25] Shu CW, Osher S. Efficient implementation of essentially non-oscillatory shock-capturing schemes, II. In: Upwind and High-Resolution Schemes. Berlin, Heidelberg: Springer; 1989, p. 328–74.
[26] Hu C, Shu CW. Weighted essentially non-oscillatory schemes on triangular meshes. J Comput Phys 1999;150(1):97–127.
[27] Balsara DS, Shu CW. Monotonicity preserving weighted essentially non-oscillatory schemes with increasingly high order of accuracy. J Comput Phys 2000;160(2):405–52.
[28] Xing Y, Shu CW. High-order well-balanced finite difference WENO schemes for a class of hyperbolic systems with source terms. J Sci Comput 2006;27(1–3):477–94.
[29] Shu CW. High order weighted essentially nonoscillatory schemes for convection dominated problems. SIAM Rev 2009;51(1):82–126.
[30] Zhang X, Shu CW. Positivity-preserving high order finite difference WENO schemes for compressible Euler equations. J Comput Phys 2012;231(5):2245–58.
[31] Li G, Lu C, Qiu J. Hybrid well-balanced WENO schemes with different indicators for shallow water equations. J Sci Comput 2012;51(3):527–59.
[32] Li G, Xing Y. High order finite volume WENO schemes for the Euler equations under gravitational fields. J Comput Phys 2016;316:145–63.
[33] Zhu J, Qiu J. A new type of finite volume WENO schemes for hyperbolic conservation laws. J Sci Comput 2017;73(2–3):1338–59.
[34] Zhu J, Shu CW. A new type of multi-resolution WENO schemes with increasingly higher order of accuracy on triangular meshes. J Comput Phys 2019;392:19–33.
[35] Zou L, Zhao H, Zhang H, Brooks CS. A Revisit to the Hicks' Hyperbolic Two-Pressure Two-Phase Flow Model (No. INL/CON-16-40382). Idaho Falls, ID (United States: Idaho National Lab.(INL); 2017.
[36] Hewitt GF, Delhaye JM, Zuber N, editors. Multiphase Science and Technology: Volume 2 (Vol. 2). Springer Science and Business Media; 2013.